Negative mobility, sliding and delocalization for stochastic networks

Dima Boriskovsky, Doron Cohen
Department of Physics, Ben-Gurion University of the Negev, Beer-Sheva 84105, Israel

We consider prototype configurations for quasi-one-dimensional stochastic networks that exhibit negative mobility, meaning that current decreases or even reversed as the bias is increased. We then explore the implications of disorder. In particular we ask whether lower and upper bias thresholds restrict the possibility to witness non-zero current (sliding and anti-sliding transitions respectively), and whether a delocalization effect manifest itself (crossover from over-damped to under-damped relaxation). In the latter context detailed analysis of the relaxation spectrum as a function of the bias is provided for both on-chain and off-chain disorder.

I. INTRODUCTION

Negative mobility, where a system responds to a perturbation in a way opposite to naive expectation, has been studied theoretically [1, 2] and experimentally [3] for numerous systems. Most examples refer to negative differential mobility (NDM) [4–8], but some also to absolute negative mobility (ANM) [8, 9]. The cited examples are in general quite complicated, and in many cases involve many-body configurations. In the present work we would like to highlight the *minimal* stochastic models where either NDM or ANM can be expected. Those are illustrated in Fig.1. In both cases the configuration reflects the existence of more than one dimension, as opposed to a simple one dimensional chain with near-neighbor transitions. The ANM configuration of Fig.1b is further characterized by a non-trivial topology: it is formally an active stochastic network that can represent the dynamics of a Janus particle [10–12] in one dimension, where the extra degree of freedom is its orientation. Clearly the discussion of NDM and ANM cannot be complete without considering the implications of disorder. Below we provide some background to the relevant literature, and further explain our motivation to deal with the prototype configurations of Fig.1.

Sliding and anti-sliding transitions.– The study of stochastic motion on a random a lattice has been introduced by Sinai [13]. In the absence of bias the spreading goes like $R \sim ln^2(t)$, where R is the distance that is covered by the particle during time t. This sub-diffusive behavior differ completely from the usual random walk result where $R \sim t^{1/2}$. Once a bias is introduced, the system exhibits a non-zero drift velocity v provided the bias exceeds a finite critical value. This is known as the *sliding transition* [14]. For sub-critical bias the spreading is $R \sim t^{\mu}$, where μ depends on the bias. Here we would like to consider the possibility that above some second critical bias the drift velocity becomes zero again. We suggest Fig.1a as the minimal configuration for such an effect. It is inspired by [15], where it has been pointed out that for a barely percolating network the transport is supported by mainly one route with numerous dangling pathways with dead ends.

Delocalization transition.– Somewhat related to the sliding transition, is the delocalization transition of the relaxation modes. Here we consider ring geometry: a chain segment with periodic boundary conditions. The delocalization transition has been discussed originally for non-Hermitian Hamiltonians [16–18], and only later for stochastic chains [19]. In this latter context "delocalization" means that the relaxation become underdamped (with oscillations). The delocalization of relaxation modes for an active network as in Fig.1b has been already studied in [20]. Here we focus on the configuration of Fig.1a, and distinguish between on-chain disorder and off-chain disorder. This part of the study is motivated by the following question: we know that in one dimension we always have localization; does it mean that in a closed ring we always have a delocalization transition?

II. THE MODEL

The particle moves on a one-dimensional lattice with dangling bonds, see Fig.1a. The dynamics is described

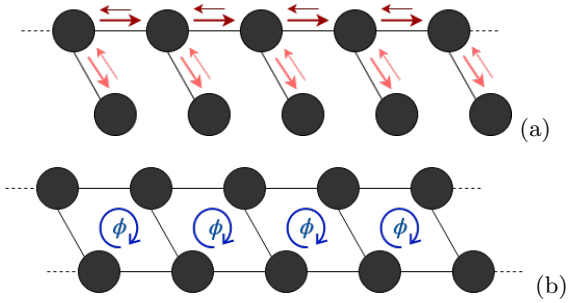

FIG. 1. **Schematic drawing of the model system.** (a) One dimensional chain with dangling bonds that serves as a minimal model for a stochastic percolating network. (b) Quasi one dimensional network that serves as a minimal model for an active gas of Janus-type particles. The parameters in panel a are: forward transition rates w_a and w_b, and backwards transition rates $w_a e^{-f}$ and $w_b e^{-\alpha f}$. The parameters in panel b include propulsion that suppresses the backward motion, namely, the rates become $w_a e^{-\phi-f}$ in the upper edges to the left, and $w_a e^{-\phi}$ in the lower edges to the right.

by a rate equation

$$\frac{d}{dt}\mathbf{p} \;=\; \boldsymbol{\mathcal{W}}\mathbf{p} \tag{1}$$

where $\mathbf{p}$ is a vector of probabilities and $\boldsymbol{\mathcal{W}}$ is a matrix of transition rates. For a non-disordered chain, by convention, all the forward rates to right are w_a, and all the outwards rates to the dangling sites are w_b. We assume bias f, and *define* the backwards transition rates as $w_a e^{-f}$ and $w_b e^{-\alpha f}$ respectively, where $\alpha > 0$ is a proportionality constant that quantifies the relative sensitivity of the dangling bonds to the bias. We emphasize that without loss of generality the forward rates, by this convention, are not affected by the bias. This helps to maintain a numerically meaningful $f \to \infty$ limit.

In Fig. 1b the particle can move either is the upper channel ($\uparrow$) or in the lower channel ($\downarrow$). It is then better to visualize the particle as an active Janus particle that can have forward or backward orientation: in the $\uparrow$ orientation it executes a stochastic propelled motion that is biased to the right, while in the $\downarrow$ orientation it executes a stochastic propelled motion that is biased to the left. Due to self propulsion there is some ratio $\exp(\phi) > 1$ between the forward and the backward motion. By our convention only the backward rates are affected by the propulsion, hence the transition rates to the left in the upper edges become $w_a e^{-\phi - f}$, and the transition rates to the right in the lower edges become $w_a e^{-\phi}$.

Different types of disorder can be introduced as discussed thoroughly for a simple chain [21], and for the configuration of Fig.1b [20]. In the present work, referring to Fig.1a, the interesting distinction is between on-chain disorder and off-chain disorder. The former adds a random component to f along the chain, while the latter is due to random α.

III. THE STEADY STATE CURRENT FOR A NON-DISORDERED CHAIN

The non-equilibrium steady state (NESS) is determined by the equation $\boldsymbol{\mathcal{W}}\mathbf{p} = 0$, which is formally a continuity equation. For the prototype percolating network of Fig. 1a, the drift velocity along the chain sites is

$$v_\uparrow \;=\; (1 - e^{-f})w_a \tag{2}$$

Without dangling bonds the occupation probability at each site of the chain is $p_{\rm chain} = 1/L$, where L is the length of the chain, hence the current is $I = (1/L)v_\uparrow$. With added dangling bonds the NESS equation implies $p_\downarrow/p_\uparrow = e^{\alpha f}$, hence

$$p_\uparrow \;=\; \frac{1}{L}\left(\frac{1}{1+e^{\alpha f}}\right) \tag{3}$$

and accordingly

$$I \;=\; p_\uparrow v_\uparrow \;=\; \frac{w_a}{L}\left(\frac{1-e^{-f}}{1+e^{\alpha f}}\right) \tag{4}$$

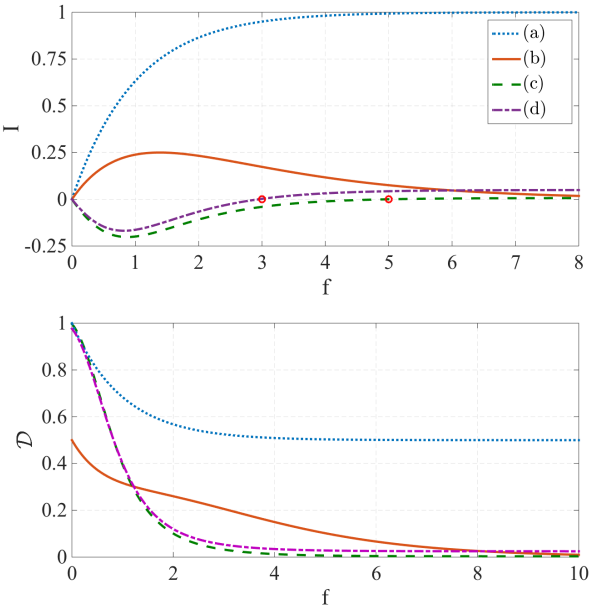

FIG. 2. **Current versus bias.** The current in units of w_a/L is plotted in the upper panel versus the bias f. The curves are for: (a) Simple chain with no dangling bonds; (b) Chain with dangling bonds ($\alpha = 1/2$). (c) Active chain with $\alpha = 2$ and $\phi = 5$. (d) Active chain with $\alpha = 2$ and $\phi = 3$. For the active chain $w_b = w_a$, and the red circles indicate the current reversal. The lower panel displays, respectively, the diffusion coefficient $\mathcal{D}$ in units of w_a.

For the prototype active network of Fig. 1b the same NESS occupation prevails, but the current becomes

$$I \;=\; p_\uparrow v_\uparrow - p_\downarrow v_\downarrow \tag{5}$$

$$\;=\; \frac{w_a}{L}\left(\frac{[1-e^{-\phi-f}] + e^{\alpha f}[e^{-\phi} - e^{-f}]}{1+e^{\alpha f}}\right) \tag{6}$$

For small f we get a linear relation $I \approx Gf$, with

$$G \;=\; \frac{w_a}{2L}\left[(1+\alpha)e^{-\phi} + (1-\alpha)\right] \tag{7}$$

We conclude that ANM will show up if $\alpha > 1$ provided the propulsion is strong enough, namely,

$$\phi \;>\; \ln\left(\frac{\alpha+1}{\alpha-1}\right) \tag{8}$$

Several I versus f plots are displayed in Fig. 2a. For completeness we also plot the diffusion coefficient $\mathcal{D}$ in Fig. 2b. The way to calculate $\mathcal{D}$ will be explained in Section V.

IV. THE STEADY STATE CURRENT FOR A DISORDERED CHAIN

We consider again the network of Fig.1a, but now with Sinai-type disorder. Recall that the NESS is determined by the equation $\boldsymbol{\mathcal{W}}\mathbf{p} = 0$, which is formally a continuity

equation. Along the n-th dangling bond it is implied that $p_{n,\downarrow}/p_{n,\uparrow} = e^{\alpha_n f}$ because the NESS current there has to be zero. Along the n-th bond of the chain we require

$$w_n^+ p_{n-1,\uparrow} - w_n^- p_{n,\uparrow} \;=\; I \tag{9}$$

If one drops the $\downarrow$ dangling sites, this equation with the normalization $\sum_n p_n = 1$ leads to a solution p_n, that is formally the identical with the solution that has been obtained by Derrida [22] for a simple ring. Namely, the current is $I = (1/L)v$, where

$$v = \left(1 - \left\langle \frac{w_n^-}{w_n^+} \right\rangle\right) \left\langle \frac{1}{w_n^+} \right\rangle^{-1} \tag{10}$$

$$= \left(1 - \frac{1}{L}\sum_n e^{-f_n}\right) w_a \tag{11}$$

This expression is valid if it gives a non-negative result. For small bias it becomes negative, indicating that $v = 0$, which is known as the *sliding transition*. If we place back the dangling sites, the solution will become $p_{n,\uparrow} = p_\uparrow p_n$, with $p_\uparrow$ that is determined by the normalization condition

$$\sum_n (1 + e^{\alpha_n f})\, p_{n,\uparrow} \;=\; 1 \tag{12}$$

The off-chain disorder α_n is assumed to be independent from the on-chain disorder. We therefore can factorize the ensemble average, and deduce that

$$p_\uparrow \;=\; \frac{1}{L}\left(\frac{1}{1 + \langle e^{\alpha_n f}\rangle}\right) \tag{13}$$

Consequently for the current we get

$$I \;=\; p_\uparrow v \;=\; \frac{w_a}{L}\left(\frac{1 - \langle e^{-f_n}\rangle}{1 + \langle e^{\alpha_n f}\rangle}\right) \tag{14}$$

This expression still features the Derrida sliding transition, but it can also provide an anti-sliding transition for large bias, if $\langle e^{\alpha_n f}\rangle$ becomes infinite. Needless to say that both the sliding and the anti-sliding transitions become sharp only in the limit of large chain ($L \to \infty$).

Both the sliding transition and the anti-sliding transition are demonstrated in Fig. 3 and Fig. 4. In Fig. 3 we assume that the f_n are box distributed within $[f - \sigma, f + \sigma]$, and that the $\alpha_n f$ are similarly distributed within $[\alpha f - \sigma, \alpha f + \sigma]$, we get

$$I \;=\; \frac{w_a}{L}\left(\frac{1 - [\sinh(\sigma)/\sigma]e^{-f}}{1 + [\sinh(\sigma)/\sigma]e^{\alpha f}}\right) \tag{15}$$

Here we have only a sliding transition because the denominator does not diverge for finite bias. In Fig.4 we assume a stretch distribution for the dangling bonds, namely, we assume that the $\alpha_n f$ have exponential distribution with an average αf. Accordingly

$$\langle e^{\alpha_n f}\rangle \;=\; \int_0^\infty e^{f'} e^{f'/(\alpha f)} df' \tag{16}$$

$$= \begin{cases} \frac{\alpha f}{1-\alpha f} & \alpha f < 1 \\ \infty & \alpha f > 1 \end{cases} \tag{17}$$

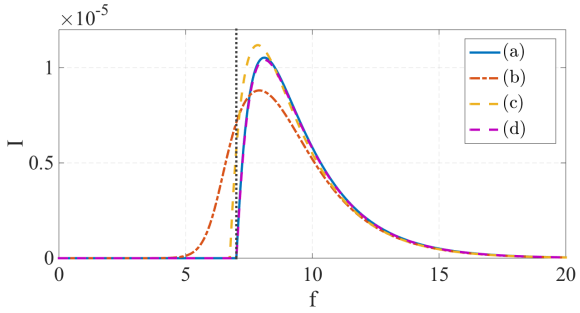

FIG. 3. **Sliding transition for a chain with dangling bonds.** The current in units of w_a/L is plotted versus the bias f with $\sigma = 10$ and $\alpha = 1/2$. (a) Analytical curve plotted by Eq.(15). (b) Numerical results with a realization of $L = 35$. (c) Analytical results evaluated by Eq. (14) with the same realization as b. (d) Analytical results evaluated by Eq.(14) with $L = 25,000$. The dotted line is $f_s \approx 7$.

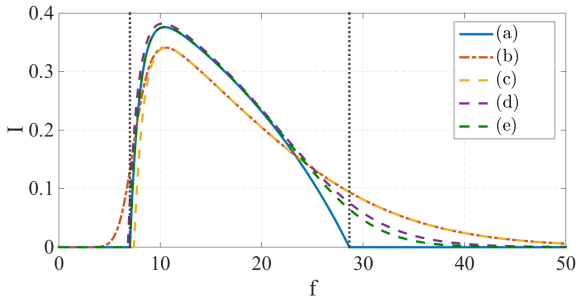

FIG. 4. **Anti sliding transitions for a chain with stretched distribution of danging bonds.** The current in units of w_a/L is plotted versus the bias f with $\sigma = 10$ and $\alpha = 0.035$. (a) Analytical curve plotted by Eq.(18). (b) Numerical results with a realization of $L = 35$. (c) Analytical results evaluated by Eq.(14) with the same realization as b. (d) Analytical results evaluated by Eq. (14) with $L = 500$. (e) Analytical results evaluated by Eq.(14) with $L = 25,000$. The dotted lines are $f_s \approx 7$ (left) and $f_c \approx 28.65$ (right).

Here the expectation values diverges for large f, and therefore for larger f the current vanishes. At the regime where the current is finite we get

$$I \;=\; \frac{w_a}{L}(1 - \alpha f)\left(1 - \frac{\sinh(\sigma)}{\sigma}e^{-f}\right) \tag{18}$$

This expression gives non-zero result within the range $f_s < f < f_c$, where

$$f_s \;=\; \ln[\sinh(\sigma)/\sigma] \tag{19}$$

$$f_c \;=\; [1/\alpha] \tag{20}$$

Again we emphasize that those sharp transitions apear only in the limit $L \to \infty$.

V. RELAXATION SPECTRUM FOR A NON-DISORDERED RING

The relaxation modes are the right eigenvectors of $\mathcal{W}$, and they satisfy the equation $\mathcal{W}\Psi = -\lambda\Psi$. In the absence of disorder, due to Bloch theorem, the matrix becomes block diagonal (see Appendix A). Consequently the eigenvalues are labelled as $\lambda_\nu(k)$, where k is the wavenumber (the Bloch phase), and $\nu = 0, 1$ is the band index. For each k we have to diagonalize a 2×2 matrix:

$$\mathcal{W}^{(k)} = \begin{pmatrix} (e^{-ik}-1)w_a^+ + (e^{ik}-1)w_a^- - w_b^+ & w_b^- \\ w_b^+ & -w_b^- \end{pmatrix} \quad (21)$$

The result of the diagonalization is demonstrated graphically in Fig.5. The NESS is the eigenstate that is associated with $\lambda_{0,0} = 0$. The two bands of the spectrum form two complex bubbles in the complex λ plane. The points are color-coded by the Bloch phase k. The second panel in Fig.5 provides further information on the polarization of the eigen-modes, which is defined as $D = |\Psi_\downarrow|^2 - |\Psi_\uparrow|^2$ (standard normalization). Note that the two bands have opposite polarity. As expected the NESS is polarized "positively" reflecting that the bias expels the probability to the dangling sites.

The boundaries of the two bands are displayed in Fig.6, and are based on the expressions that can be found in Appendix B. Our interest is mainly in the $\nu = 0$ band that is bounded from below by $\lambda = 0$. Its complexity implies under-damped relaxation in the long time limit. For large bias it becomes tiny, implying a longer relaxation time.

The weighted drift velocity can be calculated from the spectrum [23], and the result is obviously in agreement with Eq.(4). Namely,

$$v = i\frac{\partial\lambda_0(k)}{\partial k}\Big|_{k=0} = w_a\left(\frac{1-e^{-f}}{1+e^{\alpha f}}\right) \quad (22)$$

The diffusion coefficient can be calculated as well:

$$\mathcal{D} = \frac{1}{2}\frac{\partial^2\lambda_0(k)}{\partial k^2}\Big|_{k=0} \quad (23)$$
$$= \left[\frac{1+e^{-f}}{1+e^{\alpha f}}\right]\frac{w_a}{2} + \left[\frac{(1-e^{-f})^2}{(1+e^{\alpha f})^3}e^{2\alpha f}\right]\frac{w_a^2}{w_b}$$

In Fig.2b this result is displayed, and also the result for the active network (expression in Appendix B). In a simulation we can visualize the evolving probability distribution as a stretching cloud. The second term in Eq.(23), that diverges in the $w_b \to 0$ limit, reflects the departure of a drifting piece along the chain, from remnants that lags in the dangling bonds. The first term reflects the extra spreading of the drifting piece. In the zero bias limit ($f \to 0$) it is only the latter contribution that survives, leading to $\mathcal{D} \to 1/2$.

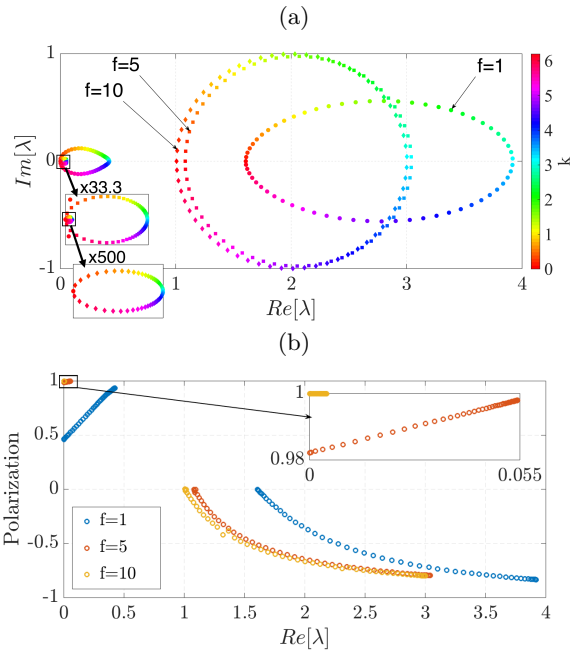

FIG. 5. **The relaxation spectrum for a non-disordered ring with dangling bonds.** In panel (a) we display in the complex plane the eigenvalues $\lambda_\nu(k)$ for a system of length $L = 100$. Here and in the next figures $w_a = w_b = 1$ and $\alpha = 1/2$. There are 3 spectra that correspond to $f = 1$ (circles), and $f = 5$ (squares), and $f = 10$ (diamonds). The points are color-coded by k. Panel (b) displays the polarization of the associated eigenmodes.

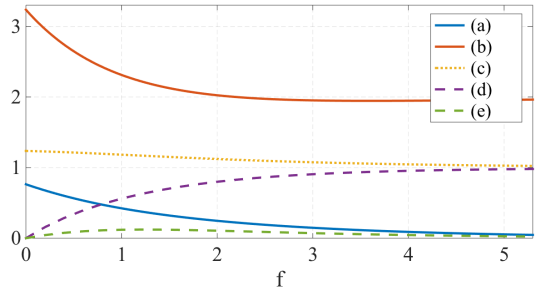

FIG. 6. **The band boundaries of the spectrum versus bias.** The boundaries of the two bands that are displayed in Fig.5 are plotted versus f: (a) $\lambda_0(\pi)$; (b) $\lambda_1(\pi) - \lambda_1(0)$; (c) $\lambda_1(0) - \lambda_0(\pi)$; (d) $\max[\mathrm{Im}(\lambda_{\nu=1})]$; (e) $\max[\mathrm{Im}(\lambda_{\nu=0})]$. The $\nu = 0$ band is responsible for the long-time under-damped relaxation. It becomes tiny for large bias, implying a longer relaxation time.

VI. RELAXATION SPECTRUM FOR A DISORDERED RING

Adding disorder some of the eigen-modes get localized, and the associated eigenvalues become real. This is demonstrated in Fig.7. Each point is color-coded by the participation number (PN), namely, the number of units cells that are occupied by the associated eigenmode.

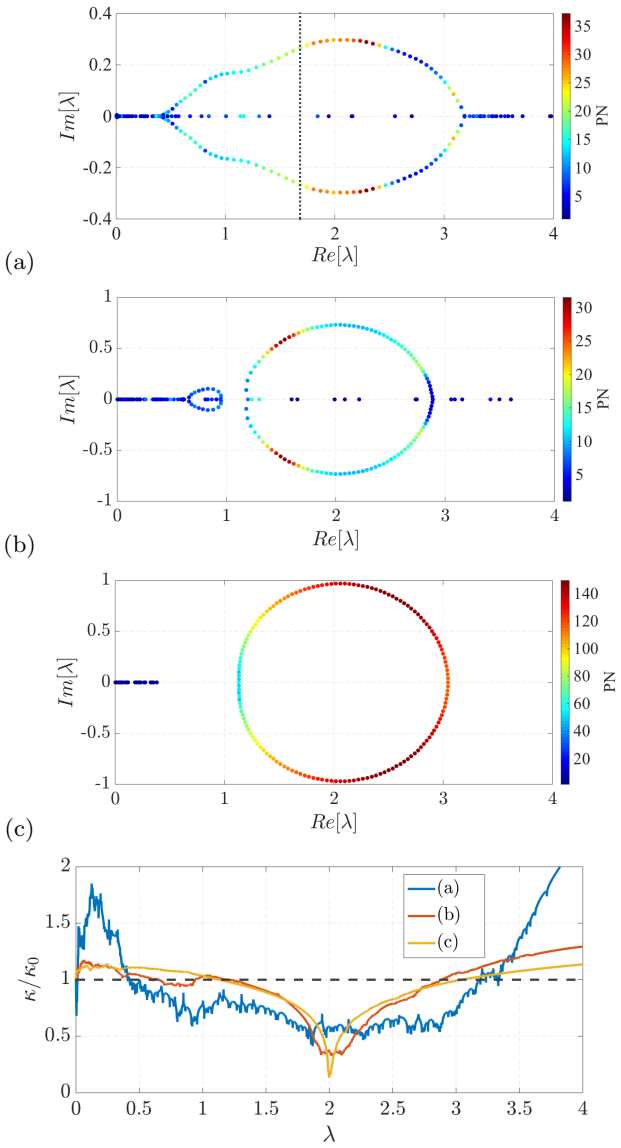

FIG. 7. **The relaxation spectrum for a disordered ring with dangling bonds.** The calculation is done for the same ring as in Fig.5, with added off-chain disorder of strength $\sigma = 5$, $L = 150$. Panels (a-b-c) are for $f = 1, 5, 10$ respectively. The points are color-coded by the participation number (PN), namely, the number of units cells that are occupied by the eigenmodes. The vertical dotted line in panels (a) is a median that divides the spectrum into two equal groups. The spectrum separates into two bands in panels (b,c).

With standard normalization the definition is

$$\mathrm{PN} = \left(\sum_n Q_n^2\right)^{-1} ; \quad Q_n = |\psi_{n\uparrow}|^2 + |\psi_{n\downarrow}|^2 \quad (24)$$

We see clearly that large PN is correlated with complexity, as expected from the general phenomenology of delocalization [18]. In the next section we shall clarify how to reduce the analysis to the familiar case. We note that the average polarization of the eigenmodes (numerical results not displayed) is similar to that of a non-disordered case (see Fig.5b).

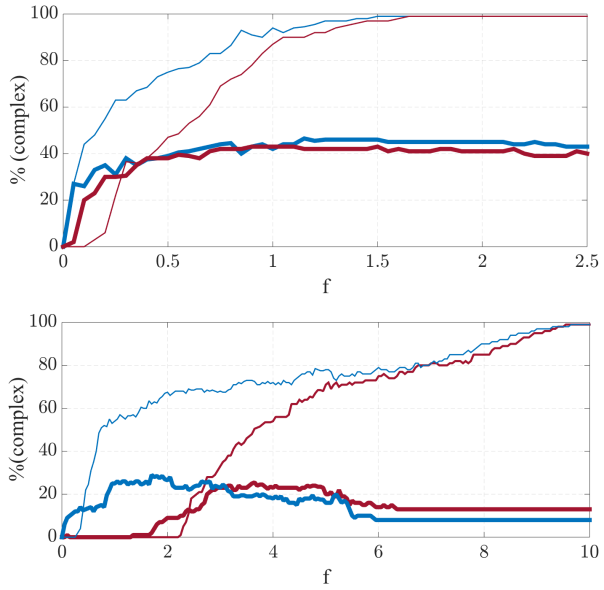

FIG. 8. **The fraction of complex eigenvalues.** The fraction is calculated separately for each band (thicker lines for $\nu = 0$). If the bands are not separated we use median for their practical definition. The upper and lower panels are for disorder of strength $\sigma = 1, 5$ respectively. Both off-chain (blue) and on-chain (red) disorder are considered. For on-chain disorder the delocalization transition is clearly resolved for $\sigma = 5$, while for off-chain disorder the $\nu = 0$ band always feature a complex bubble. For strong bias the $\nu = 0$ band exhibits complexity saturation, while the $\nu = 1$ band becomes 100% complex irrespective of the disorder type.

Fig.8 displays the fraction of complex eigenvalues. The fraction is calculated separately for each band. If the bands are not separated by a gap, we use median for their practical definition. Namely, 50% of the eigenvalues that have the lowest Re[λ] are defined as the $\nu = 0$ band, bounded from above by a vertical dotted line in Fig.7a. For on-chain disorder the delocalization transition is clearly resolved if the disorder is strong enough. Namely, up to some critical value of f the complex bubble that touches the origin disappears, and the eigenvalues there become real. Complex eigenvalues with large Re[λ] may exist: they represent a transient under-damped relaxation. For long times the predominant dynamical behavior is over-damped if the bias is below the delocalization threshold. We see that such delocalization transition does not appear if we have only off-chain disorder. In the latter case a small complex bubble that touches the origin survives even if the disorder is large, irrespective of the bias. For strong bias the $\nu = 0$ band exhibits complexity saturation, meaning that a finite fraction of real eigenvalues survives. This complexity saturation will be explained by reduction to the standard case (see next section). In contrast the $\nu = 1$ band becomes 100% complex irrespective of the disorder type.

VII. THE LOCALIZATION OF THE EIGEN-MODES

In order to understand the delocalization transition for on-chain disorder, and its absence for off-chain disorder, we show that the analysis of the characteristic equation, $\det(\lambda + \boldsymbol{\mathcal{W}}) = 0$, can be reduced to the well studied "standard model". The latter term refers to a simple single channel tight binding model with near-neighbor transitions.

The equation for eigenmodes $\boldsymbol{\mathcal{W}}\psi = -\lambda\psi$ for a chain with dangling bonds is

$$w_n^+\psi_{n-1} + w_{n+1}^-\psi_{n+1} + c_n^-\psi_{n,\downarrow} - \gamma_n\psi_n = -\lambda\psi_n$$
$$c_n^+\psi_n - c_n^-\psi_{n,\downarrow} = -\lambda\psi_{n,\downarrow}$$

where we used the simplified notations $\psi_n \equiv \psi_{n,\uparrow}$, and $w_n^\pm$ for the forward and backward rates along the chain, and $c_n^\pm$ for the forward and backward rates along the dangling bonds, and $\gamma_n = w_{n+1}^+ + w_n^- + c_n^+$. Expressed in terms of parameter that have been defined in Fig.1a:

$$w_n^+ = w_a \tag{25}$$
$$w_n^- = w_a e^{-f_n} \tag{26}$$
$$c_n^+ = w_b \tag{27}$$
$$c_n^- = w_b e^{-\alpha_n f} \tag{28}$$

In the numerical demonstrations we assume that for the f_n are box distributed within $[f-\sigma, f+\sigma]$ for on-chain disorder, and that the $\alpha_n f$ are similarly distributed within $[\alpha f - \sigma, \alpha f + \sigma]$ for off-chain disorder. Eliminating the dangling bonds from the set of coupled equations we get the single-channel tight binding equation

$$w_n^+\psi_{n-1} + w_{n+1}^-\psi_{n+1} - u_n(\lambda)\psi_n = -\lambda\psi_n \tag{29}$$

with

$$u_n(\lambda) \equiv [w_{n+1}^+ + w_n^- + c_n^+] - \frac{c_n^+ c_n^-}{c_n^- - \lambda} \tag{30}$$
$$\approx (1 + e^{-f_n})w_a - \lambda\, e^{\alpha_n f} \tag{31}$$

The second line above is a small λ expansion. We see that off-chain disorder (random α_n) introduces diagonal disorder of intensity that is proportional to λ^2, while on-chain disorder (random f_n) does not vanish in this limit. This already explains qualitatively why the λ spectrum is hardly affected by off-chain disorder in the vicinity of the origin.

We proceed with a quantitative treatment of the characteristic equation $\det(\lambda + \boldsymbol{\mathcal{W}}) = 0$. After the reduction to a single-channel tight binding model it takes the form $\det(\lambda + \boldsymbol{W}) = 0$, where $\boldsymbol{W}$ corresponds to Eq.(29). For the calculation of the determinant it is convenient to write the forward and backward rates as $w_n \exp(\pm f_n/2)$, where

$$w_n \equiv \sqrt{w_n^+ w_n^-} = w_a \exp(-f_n/2) \tag{32}$$

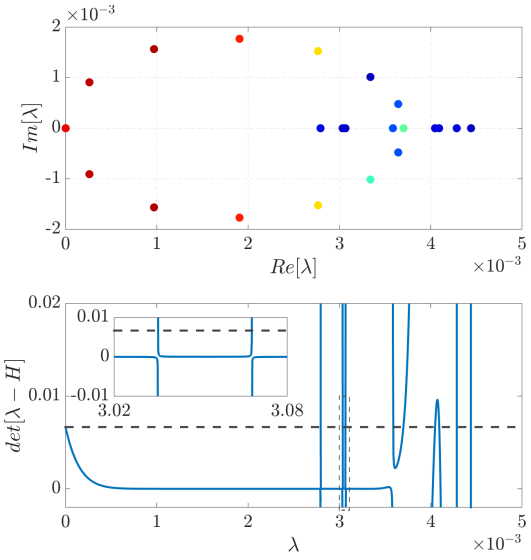

FIG. 9. **Spectral determinant for off-chain disorder.** We consider an $L = 150$ chain with off-chain disorder $\sigma = 5$ and $f = 2$. We focus on the λ-region where we have both complex and real eigenvalues in the $\nu = 0$ band. The inset zooms the indicated region where two real eigenvalues are barely resolved.

The affinity is defined as $\sum_n f_n = Nf$, where f is what we called "bias". Then it is possible to define an associated hermitian matrix $-\boldsymbol{H}$ that has the same diagonal elements, while the off-diagonal couplings are w_n. A linear-algebra formula [13] (optionally see Appendix C of [12]) leads to the identity

$$\det(\lambda + \boldsymbol{W}) = \det(\lambda - \boldsymbol{H}) - \left[e^{Nf/2} + e^{-Nf/2} - 2\right]\prod_n(-w_n) \tag{33}$$

Hence the characteristic equation takes the form:

$$\prod_{k=0}^{N}\left(\frac{\lambda - \epsilon_k(\lambda; f)}{-w_{\rm avg}}\right) = 2\left[\cosh\left(\frac{Nf}{2}\right) - 1\right] \tag{34}$$

where ϵ_k are the real eigenvalues of the hermitian $\boldsymbol{H}$ matrix, and

$$w_{\rm avg} = \left[\prod_{n=0}^{N} w_n\right]^{1/N} \tag{35}$$

A numerical demonstration of this (exact) equation is provided in Fig.9. Whenever it is satisfied, a real root is found. Singularities that are implied by Eq.(30) are an artefact that can be ignored.

The log of the left hand side in Eq.(34), after dividing by N, is the Thouless formula for the inverse localization length κ in the hermitian problem. Consequently, taking into account that $\lambda = 0$ is a root, the characteristic equation can be written as

$$\kappa(\lambda) = \kappa(0) \tag{36}$$

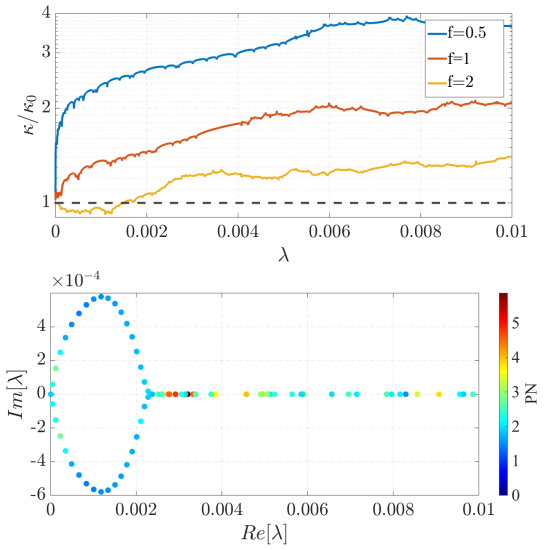

FIG. 10. **The inverse localization length for on-chain disorder.** We consider an $L = 300$ chain with both off-chain and on-chain disorder $\sigma = 5$. The inverse localization length $\kappa(\lambda)$ of Eq.(37) is calculated in the λ range of the $\nu = 0$ band. The bias $f = 0.5, 1, 2$ is indicted in the legend. In the lower panel we display the spectrum for $f = 2$. The spectrum is complex in the range where $\kappa(\lambda) < \kappa(0)$.

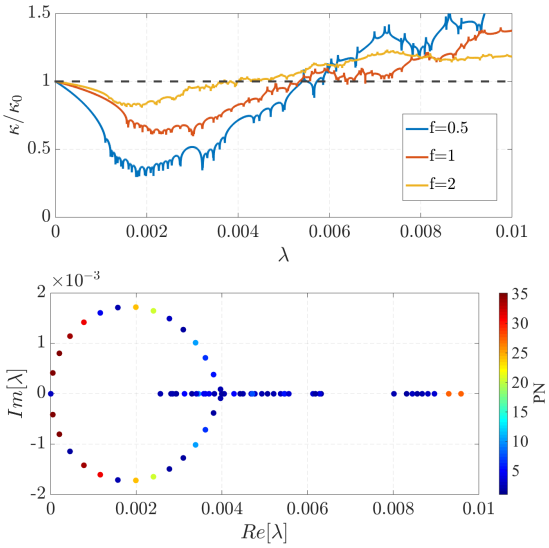

FIG. 11. **Inverse localization length for off-chain disorder.** The same as for Fig.10, but with only off-chain disorder. Here the spectrum has a complex fraction for any f.

Substitution of the definition of w_n leads to

$$\kappa(\lambda) = \frac{f}{2} + \frac{1}{N}\sum_{k=0}^{N} \ln\left|\frac{\lambda - \epsilon_k(\lambda; f)}{w_a}\right| \qquad (37)$$

A few words are in order regarding the use of this formula. First of all it really has the meaning of an inverse localization length in the range where the (real) spectrum stretches, otherwise it is a formal continued expression. It is implicit that we refer here to the envelope of the spectral determinant. Traditionally κ is determined using a transfer matrix method. There are also some analytical approximations that can be used (see next paragrpah). But for our purpose a direct numerical calculation using the Thouless formula is most convenient. Note that for any λ we have to calculate again the $\epsilon_k(\lambda; f)$ spectrum, unlike the "standard model" where $\boldsymbol{H}$ is λ independent. The reduction of the $\boldsymbol{\mathcal{W}}$-problem to the $\boldsymbol{H}$-problem assumes real λ, hence Eq.(36) provides real roots if $\kappa(\lambda) > \kappa(0)$, otherwise complex spectrum should appear (which cannot be extracted directly by inspection). This expectation is confirmed numerically by Fig.10 and Fig.11.

As mentioned above, there are some analytical approximations that can be used in order to evaluate κ. Exact results are available in the continuum limit, which is not useful here. We are therefore satisfied with a standard Born-approximation that is based on a Fermi-Golden-Rule picture:

$$\kappa(\lambda) = \frac{\sigma_\parallel^2}{8\bar{w}^2 k_\lambda^2} + \frac{\sigma_\perp^2}{8\bar{w}^2} k_\lambda^2 \qquad (38)$$

Those are Eqs(14-15) of [14], where further refinements are discussed, and additional references therein. This equation requires a careful explanation. It is expressed in terms of the wavenumber that is determined by the dispersion relation $\lambda = 2\bar{w}(1 - \cos(k))$, where $\bar{w}$ is the harmonic average over the bond couplings Eq.(32). The approximation $\lambda \approx w_a k^2$ can be used for weak disorder in the small wavelength regime. The two terms in Eq.(38) correspond to on-diagonal and off-diagonal disorder respectively. We discuss the two terms separately below.

The *off-diagonal disorder*, aka resistor network disorder, is the same type of disorder that appears e.g. in the Debye model (balls connected by springs). The strength of this disorder is defined as follows:

$$\sigma_\perp^2 \equiv \bar{w}^4 \mathrm{Var}\left[\frac{1}{w_n}\right] \approx \frac{1}{4} w_a^2 e^{-f} \mathrm{Var}[f_n] \qquad (39)$$

This definition assumes that the bonds are uncorrelated. The approximation is based on first order treatment of the disorder in Eq.(32). Looking at Eq.(38) we see that its effect is significant for the short-wavelength modes, and can be neglected in the vicinity of $\lambda = 0$. It is the same as in the Debye model where it is argued that the long-wavelength modes tend to be extended.

The *on-diagonal disorder* is more subtle. In the standard Anderson model all bonds are identical and it is common to consider white on-site disorder. Here it is not the case, hence the definition for the strength of the disorder becomes more subtle:

$$\sigma_\parallel^2 \equiv \mathrm{Var}_\lambda\left[u_n - w_n - w_{n-1}\right] \qquad (40)$$

If $\boldsymbol{H}$ were a stochastic kernel that preserve probability, then we would get from this expression $\sigma_\parallel = 0$, and would

be left with Debye-type localization only. But this is not the case here. We have extra diagonal disorder analogous to pinning of the balls to the ground in the Debye model. This extra disorder leads to Anderson-type localization at the vicinity of $\lambda = 0$. The second issue to notice is the subscript in Var_λ. This subscript reminds us that the diagonal elements are not independent random variables. Consequently we do not have "white disorder" and the variance has to be calculated at the "energy" of interest. Namely, the Born approximation Eq.(38) is based on evaluation of matrix elements $\langle -k|U(x)|k\rangle$ for backscattering. Here we use for clarity continuous space notations (x instead of n). Averaging the squared matrix elements over realizations of the potential $U(x)$ one deduces that

$$\mathrm{Var}_\lambda[U(x)] \;=\; \sum_r e^{ikr} C(r) \tag{41}$$

where $C(r)$ is the correlation function of the disorder. Here we are back with discrete notions, accordingly the distance r between sites is an integer number. For "white" disorder $C(r) = \mathrm{Var}(U_n)\delta_{r,0}$. But the potential U_n in the square brackets if Eq.(40) is correlated. For presentation purpose we assume also $f \ll 1$, which corresponds to the continuum limit, while the more general case is addressed in Appendix C. The disorder in leading order comes out

$$U_n = -\frac{w_a}{2}(f_n - f_{n-1}) - \lambda f \alpha_n + \mathrm{const} \tag{42}$$

Consequently we obtain

$$\sigma_\parallel^2 \;\approx\; \frac{w_a}{4}\lambda \mathrm{Var}[f_n] + \lambda^2 f^2 \mathrm{Var}[\alpha_n] \tag{43}$$

Substitution into Eq.(38) we see, as anticipated, that off-chain disorder provides a contribution proportional to λ that always vanishes in the vicinity of $\lambda = 0$, while on-chain disorder does not vanish.

The bottom line is very simple, and we summarize it in simple words: the inverse localization length is determined by the effective diagonal disorder. The strength of this disorder is proportional to λ^2 for off-chain disorder, and therefore we always get a complex bubble at the vicinity of the origin, indicating under-damped relaxation. For on-chain disorder the inverse localization length approach a finite value at the limit $\lambda \to 0$. Therefore the complexity depends on the slope $\kappa'(0)$ at the origin. This slope becomes negative for large enough f, hence we get a delocalization transition. The details in the latter case are the same as in the "standard model", see [10] where also the complexity saturation is explained.

VIII. SUMMARY

Stochastic networks are of general interest in many fields of Physics, as well as in Chemistry and Engineering. Key questions in the study of such networks are how they respond to bias, and what are their relaxation modes. In the traditional studies of tight binding models the main observations have to do with the sliding and the delocalization transitions. Once we allow more complex quasi-one-dimensional configurations, some new issues emerge. Here we highlight the theme of negative mobility (NDM/ANM) and the effect of on-chain and off-chain disorder. Our main observations are: **(a)** The minimal configuration for NDM is Fig.1a that features dangling bonds with dead-end. The dependence of the current on the bias is demonstrated in Fig.4. **(b)** The minimal configuration for ANM requires an active network, as in Fig.1b. The dependence of the current on the bias is demonstrated in Fig.2. **(c)** Additional ingredient that is required in order to get an anti-sliding effect that suppresses the current for large bias, is a wide distribution of dangling pathways. This is demonstrated in Fig.4. **(d)** Off chain disorder leads to localization that is not strong enough to induce over-damped relaxation, hence delocalization transition is absent. In the latter context it is implied that also sliding transition does not take-place. In fact the absence of sliding transition is much easier for understanding because for off-chain disorder activation barriers are not formed. We have explained how the analysis of the relaxation spectrum can be carried out using a reduced tight binding model and known results for the calculation of the inverse localization length.

Acknowledgment.– This research was supported by the Israel Science Foundation (Grant No.283/18).

Appendix A: The Bloch matrix

For a one dimensional chain with dangling bonds, in the absence of disorder, the matrix $\boldsymbol{\mathcal{W}}$ can be written using momentum and spin operators. For symmetric transitions

$$\boldsymbol{\mathcal{W}} \;=\; w_b[\boldsymbol{\sigma}_x - 1] + \sum_{\pm} \boldsymbol{\sigma}_{\uparrow} w_a [e^{\pm i\mathbf{p}} - 1] \tag{A1}$$

where $\boldsymbol{\sigma}_{\uparrow}$ is a projector on the chain sites, while the Pauli operator $\boldsymbol{\sigma}_x$ induce transitions between $\uparrow$ and $\downarrow$ sites. The momentum with eignevalue k is a constant of motion, and therefore the matrix is composed into blocks:

$$\boldsymbol{\mathcal{W}}^{(k)} = \begin{pmatrix} -w_b^+ + (e^{-ik}-1)w_a^+ + (e^{ik}-1)w_a^- & w_b^- \\ w_b^+ & -w_b^- \end{pmatrix} \tag{A2}$$

In the latter expression we have assumed that transitions do not have the same rates in the forward and in the backward directions, leading to an asymmetric non-hermitain matrix.

For a quasi one dimensional active network we add the transitions along the $\downarrow$ sites and get

$$\boldsymbol{\mathcal{W}}^{(k)} = \begin{pmatrix} -w_b^+ + (e^{-ik}-1)w_{a\uparrow}^+ + (e^{ik}-1)w_{a\uparrow}^- & w_b^- \\ w_b^+ & -w_b^- + (e^{-ik-1})w_{a\downarrow}^+ + (e^{ik}-1)w_{a\downarrow}^- \end{pmatrix} \tag{A3}$$

Appendix B: Band boundaries

The expressions for the band boundaries, assuming $w_a = w_b = 1$ are:

$$\lambda_0(\pi) = \frac{1}{2} e^{-(1+\alpha)f} \left[e^f + 2e^{\alpha f} + 3e^{(1+\alpha)f} + \sqrt{e^{2f} + 4e^{2\alpha f} + 9e^{2(1+\alpha)f} - 2e^{(2+\alpha)f} - 4e^{(1+\alpha)f} + 12e^{(1+2\alpha)f}} \right] \tag{B1}$$

$$\lambda_1(0) = 1 + e^{-\alpha f} \tag{B2}$$

$$\lambda_1(\pi) = \frac{1}{2} \left[3 + 2e^{-f} + e^{-\alpha f} - e^{(1+\alpha)f} \sqrt{e^{2f} + 4e^{2\alpha f} + 9e^{2(1+\alpha)f} - 2e^{(2+\alpha)f} - 4e^{(1+\alpha)f} + 12e^{(1+2\alpha)f}} \right] \tag{B3}$$

The full expression for $\lambda_0(k)$ is not too illuminating, and therefore is not displayed. Its second derivative at $k = 0$ gives the diffusion coefficient $\mathcal{D}$ of Eq.(23) which is plotted in Fig.2b. For completeness we write also what is result for the diffusion coefficient for the active network:

$$\mathcal{D} \;=\; \left[\frac{(1 + e^{\alpha f - f}) + e^{-\phi}(e^{-f} + e^{\alpha f})}{1 + e^{\alpha f}} \right] \frac{w_a}{2} + \left[\frac{e^{2\alpha f}(1 + e^{-f})^2 (1 - e^{-\phi})^2}{(1 + e^{\alpha f})^3} \right] \frac{w_a^2}{w_b} \tag{B4}$$

Appendix C: The on-diagonal disorder

We write the bias for a chain bond $f_n = f + \tilde{f}_n$, and for a dangling bond $\alpha_n = \alpha + \tilde{\alpha}_n$. Accordingly we have for weak disorder, after dropping a constant,

$$U_n \;\approx\; -\frac{w_a}{2} e^{-f/2} \left[(2e^{-f/2} - 1)\tilde{f}_n - \tilde{f}_{n-1} \right] - \lambda f e^{\alpha f} \tilde{\alpha}_n \;\equiv\; A\tilde{f}_n + B\tilde{f}_{n-1} + C\tilde{\alpha}_n \tag{C1}$$

Consequently we get for the effective strength of the disorder

$$\sigma_{\parallel}^2 \;\approx\; [A^2 + B^2 + 2AB\cos(k)]\mathrm{Var}[f_n] + C^2 \mathrm{Var}[\alpha_n] \tag{C2}$$

In the main text we have highlighted the continuum limit ($f \ll 1$) for which $A \approx -B$, and $\cos(k) \approx 1 - (1/2)k^2$, and therefore the first term is proportional to λ. In general we might have a term that does not vanish in the limit $\lambda \to 0$. Then one has to use a formula that goes beyond the diverging FGR approximation of Eq.(38).

[1] J. Cividini, D. Mukamel & H. A. Posch, Journal of Physics A 51, 8 (2018).
[2] R. K. P. Zia, E. L. Praestgaard & O. G. Mouritsen, American Journal of Physics 70, 4 (2002).
[3] H. Bottger & V. V. Bryksin, Physica Status Solidi (b) 113, 1 (1992).
[4] E. M. Conwell, Physics Today 23, 6, 35 (1970).
[5] F. Nava, C. Canali, F. Catellani, G. Gavioli & G. Ottaviani, J. of Phys. C 9, 9 (1976).
[6] C. J. Stanton, H. U. Baranger & J. W. Wilkins, Applied Physics Letters 49, 3 (1986).
[7] X. L. Lei, N. J. M. Horing & H. L. Cui, Phys. Rev. Lett. 66, 25 (1991).
[8] A. Sarracino, F. Cecconi, A. Puglisi & A. Vulpiani, Phys. Rev. Lett. 117, 17 (2016).
[9] B. J. Keay, S. Zeuner, S. J. Allen, K. D. Maranowski, A. C. Gossard, U. Bhattacharya & M. J. W. Rodwell, Phys. Rev. Lett., 75, 22 (1995).
[10] A. Walther & H. E. A. Muller, *Janus Particle Synthesis, Self-Assembly and Applications*, p.1-28 (2012).
[11] P. M. Wheat, N. A. Marine, J. L. Moran & J. D. Posner, Langmuir 26, 13052 (2010).
[12] A. M. Menzel, Phys. Rep. 554, 1 (2015).
[13] Ya. G. Sinai, Theory Probab. Appl. 27(2), 256-268 (1980).
[14] B. Derrida & Y. Pomeau, Phys. Rev. Lett. 48, 9 (1982).
[15] G. Ben Arous & A. Fribergh, arXiv preprint arXiv:1406.5076 (2014).
[16] N. Hatano & D. R. Nelson, Phys. Rev. Lett. 77, 3 (1996).
[17] N. Hatano & D. R. Nelson, Phys. Rev. B 56, 8651 (1997).
[18] N.M. Shnerb, D.R. Nelson, Phys. Rev. Lett. 80, 5172 (1998).
[19] D. Hurowitz & D. Cohen, Phys. Rev. E 93, 6 (2016).
[20] D. Shapira, D. Meidan & D. Cohen, Phys. Rev. E 98, 1 (2018).
[21] D. Hurowitz & D. Cohen, Scientific Reports 6(1) (2015).
[22] B. Derrida, Journal of Statistical Physics 31, 3 (1983).
[23] D. Hurowitz & D. Cohen, Phys. Rev. E 90, 032129 (2014).
[24] L. G. Molinari, Linear Algebra Appl. 429, 2221 (2008).
[25] I. Weinberg, Y. de Leeuw, T. Kottos & D. Cohen, Phys. Rev. E 93, 6 (2016).